Electrochimica Acta 87 (2013) 473–488

Contents lists available at SciVerse ScienceDirect

Electrochimica Acta

journal homepage: www.elsevier.com/locate/electacta

Comparison of commercial battery cells in relation to material properties

Grietus Mulder[a,b,f,*], Noshin Omar[b,c], Stijn Pauwels[d], Marcel Meeus[e], Filip Leemans[a,f], Bavo Verbrugge[b,1], Wouter De Nijs[d], Peter Van den Bossche[c], Daan Six[a,f], Joeri Van Mierlo[b]

[a] Vlaamse Instelling voor Technologisch Onderzoek, Unit Energy Technology, Mol, Belgium
[b] Vrije Universiteit Brussel, Mobility and Automotive Technology Research Group, Brussels, Belgium
[c] Erasmus Hogeschool Brussel, Department Industrial Sciences and Technology, Brussels, Belgium
[d] Flanders' DRIVE, Lommel, Belgium
[e] Umicore, Research and Development, Olen, Belgium
[f] EnergyVille, Genk, Belgium

ARTICLE INFO

Article history:
Received 13 June 2012
Received in revised form
13 September 2012
Accepted 16 September 2012
Available online 8 October 2012

Keywords:
Automotive
Electric vehicles
Lithium-ion battery
Nickel-metal hydride battery
Test methods
Cell characterisation

ABSTRACT

This article evaluates the behaviour of lithium-ion cells of several chemistries and one nickel-metal hydride cell for automotive applications like (plug-in) hybrid vehicles and battery electric vehicles. The evaluation is based on an enhanced test methodology that enables the comparison of cell behaviour. Tests for high power and high energy application have been integrated. The characterisation tests exist of four test methods. The tests make large differences visible between the cell species. The 5 C efficiency for example is between 75 and 90% while the cell temperature varies from 29 to 52 °C. The power density is 80 W/kg for the NiMH cell and lies between 330 and 3100 W/kg for the lithium-ion cells. The cell results have been brought into relation to the material properties, the shape, referring to existing literature. The test plan made it possible to make an initial division in the cells. It appears that the manufacturer's knowhow is more important than the general electrode classification to produce outstanding cells.
© 2012 Elsevier Ltd. All rights reserved.

1. Introduction

In Belgium a consortium of twelve companies and research faculties tied together to find the optimal battery cells on the market in order to develop a complete battery system [1]. The research focussed on diverse automotive applications, ranging from hybrid electric cars with a battery of 3 kW h up to battery electric cars with a battery of 25 kW h. This means that both high power and high energy applications are foreseen. The test results should be able to distinguish the good battery cells for either application.

In order to find the optimal cells from which battery packages can be made, two types of test regimes have been foreseen:

- characterisation tests;
- lifetime tests.

Although the lifetime tests are most important to experience whether cells are suited for their ultimate task, characterisation tests are needed to find the better cells, to separate them in high power and high energy application, and to find the individual key strength. Other test methods like reliability tests and abuse tolerance tests, like proposed in [2,3], are not foreseen within this phase.

This article evaluates the results of the characterisation tests, based on a previously developed enhanced test methodology [4]. This method has been developed to obtain results that allow good comparison of the cells and to speed up the tests. Also, the charging behaviour of cells is underexposed in the existing standards.

The article starts with the intended applications and the cell properties according to the manufacturer, followed by a materials description to understand better the observed battery behaviour

Abbreviations: C-rate, current relative to the capacity of a cell or battery. The capacity is the 1 h capacity, i.e. the capacity derived from of a full discharge in 1 h (C or A/A h); C3-rate, The capacity is the 3 h capacity, i.e. the capacity derived from of a full discharge in 3 h (C3); cap., cell capacity (A h); c_p, specific heat capacity; DOD, depth of discharge (%); BEV-PC, battery electric personal car; HEV-B, hybrid electric bus; HEV-PC, hybrid electric personal car; HPPC, hybrid pulse power characterisation test; I_{max}, maximum allowed current by the manufacturer; I_T, current relative cell or battery capacity as declared by the manufacturer (I_T or A/A h); LFP, lithium-ion iron phosphate cell; LMO, lithium-ion manganese oxide cell; LNO, lithium-ion nickel oxide cell; LTO, lithium-ion titanate oxide anode; NCA, lithium nickel cobalt aluminium oxide cell; NiMH, nickel-metal hydride cell; NMC, lithium-ion nickel cobalt manganese oxide cell; OCV, open circuit voltage; PHEV-PC, plug-in hybrid personal car; R, resistance (mΩ); RT, room temperature; SEI, surface-electrode interface; SOC, state of charge (%); V_{avg}, average cell potential (V).

* Corresponding author at: Vlaamse Instelling voor Technologisch Onderzoek, Unit Energy Technology, Mol, Belgium. Tel.: +32 14 33 58 59.
E-mail address: Grietus.Mulder@vito.be (G. Mulder).
[1] Current address: Belgian Defence, Brussels, Belgium.

0013-4686/$ – see front matter © 2012 Elsevier Ltd. All rights reserved.
http://dx.doi.org/10.1016/j.electacta.2012.09.042

Table 1
Battery requirements for the selected 4 automotive applications.

Vehicle type	HEV-PC	HEV-B	PHEV-PC	BEV-PC
Voltage (V)	300	600	300	300
Stored energy (kW h)	3	18	10	25
Max. charging power (kW)	24	48	24	24
Max. discharging power (kW)	45	120	60	60
Battery size (A h)	10	30	33	83
Max. charging current (A)	80	80	80	80
Max. discharging current (A)	150	200	200	200
C-rate charging (C)	8	2.7	2.4	1.0
C-rate discharging (C)	15	6.7	6.0	2.4

mainly in comparison to the cathode composition and shape. The test results are dealt with per cathode chemistry (individual test results section) and compared to each other in the next section. A discussion follows on the behaviour of the cells and an evaluation of the test method [4] is made.

2. Intended applications and basic cell properties

To evaluate existing characterisation tests, it is necessary to have insight in the demands imposed by the intended applications and in the basic properties of the cells to be tested according to their data sheets. This is necessary as the proposed tests should fit with the anticipated applications, but also take into account the characteristics of the cells that will be tested.

The consortium agreed on 4 applications: hybrid electric car (HEV-PC), hybrid electric bus (HEV-B), plug-in hybrid electric car (PHEV-PC) and battery electric car (BEV-PC). A short outline of the requirements is given in Table 1. The basic properties are total battery system voltage, the energy to be stored and the (dis)charge power. From these figures an impression can be obtained of the battery size expressed in ampere hours (A h) and in C-rates for charging respectively discharging. Normally, the C-rate is derived by the actual current in ampere and the actual cell or battery capacity in A h. In the table the needed current is simply divided by the needed battery size. The selected applications need a charge C-rate between 1 and 8 as well as a discharge C-rate between 2 and 15.

The objective is to test both lithium-ion cells of several chemistries and nickel-metal hydride cells given that the latter are the reference and will play in the near future an important role for automotive applications. 13 different cells have been obtained and tabulated in Table 2. The table provides a short list of properties of the cells that are important to consider for the appropriateness of the characterisation tests and the appropriateness for the applications. The cells have been arranged by chemistry and cell size. 9 of the 13 cells are lithium-ion iron phosphate cells (LFP). Further, there is one lithium nickel cobalt aluminium oxide cell (NCA), two lithium-ion nickel cobalt manganese oxide cells (NMC) and one nickel-metal hydride cell (NiMH).

The cells show a wide variety in shapes and connection methods. These characteristics are important for the mechanical integration of the cells in a battery package. They can also have an influence on the weight density and the temperature performance. Although most of the cylindrical cells have a modest capacity (around 3 A h) in comparison with the intended application, they constitute the largest actual market share.

Cell manufacturers provide often the (dis)charge rates expressed in ampere. Since all cell capacities are unequal, it is better to express the (dis)charge rates as a C-rate. In the table the C-rate is obtained by simply dividing the announced current by the capacity according to the manufacturer. The (dis)charge rates in Table 2 have been split up in four categories: recommended rate, maximum rate, recommended pulse rate and maximum

Table 2
Cell specifications according to manufacturers.

	Cell information					Charging information					Discharging information						Other information			
ID	Cathode	Shape	Connection	Capacity		Recomm. cont.	Max.	Max. pulse			Recomm. cont.	Max. cont.	Recomm. pulse	Max. pulse	Pulse period	Max. temp.	Resistance	Cycles (80% DOD)	Price	
	(–)	(–)	(–)	A h	@ C (–)	C-rate (–)	C-rate (–)	C-rate (–)	(s)	(°C)	C-rate (–)	C-rate (–)	C-rate (–)	C-rate (–)	(s)	(°C)	(mΩ)	(–)	(€/kW h)	
A	NCA	Cylinder	Screw	27	0.2	1	4		6 15	40	2	10		28	2	60	0.5	>1000	823	
B	NMC	Pouch	Flap	70	0.5	0.5	2			45	0.1	5	1	8	10	55	0.5	1200	417	
C	NMC	Pouch	Flap	12	0.5	0.5	3			45	0.5	18	9	23	10	55	0.9	1200	811	
D	LFP	Prismatic	Screw	45	0.5	0.5				60		10				70		>1000		
E	LFP	Pouch	Flap	40	0.2	0.5	2			45	1	10				60	2	1500		
F	LFP	Prismatic	Screw	30	1	0.5				60		10				70		>1000		
G	LFP	Pouch	Flap	14		0.5				40		10		20	10	50				
H	LFP	Pouch	Flap	10	1		3	6	?	45		20		40	?	65	2	1000	296	
I	LFP	Cylinder	Screw	10	0.2		3			45		8		20	1	75				
J	LFP	Cylinder	Side	3.5	0.2	1	2			45		10				45	10			
K	LFP	Cylinder	Side	2.5	0.2	0.2	0.5			45	6	6		20	?	60	15	2000		
L	LFP	Cylinder	Side	2.3		1	4			60	30			52	10	60	8	>1000		
M	NiMH	Prismatic	Screw	30	0.2	0.5				45		2				50	12	>1500		

pulse rate. No information was provided on the recommended charge pulses. So, this column has been left out of the table. For the pulse rates also the pulse duration should be given. However, the manufacturers do not always provide these data. The table makes also clear that more data is provided on discharging than on charging cells.

The continuous discharge rate is between 5 C (1 cell) and 20 C (1 cell) and even 30 C (1 cell) for lithium-ion cells and 2 C for the NiMH cell. 7 cells can withstand at least 20 C pulses, with a duration varying from 1 s up to continuous. A continuous 20 C discharge means that a cell is empty in 3 min... The maximum allowable temperature for discharge is in between 45 and 75 °C.

The continuous charge rate is between 0.5 C (1 lithium-ion cell and the NiMH cell) and 4 C (2 cells). Only two manufacturers give information on charging with a pulse, of which one is not offering the duration. This general lack of pulse charge information is striking, as it is an important parameter for regenerative braking in vehicle applications. The maximum allowable temperature for charging cells is almost always lower than for discharging and is in between 45 and 60 °C.

Some conclusions can be drawn confronting Table 1 with 2. It can be deduced that the 15 C discharge demand for HEV-PC can be fulfilled by 3 cells under continuous conditions and by 7 cells under pulse condition. However, the 8 C charging for the HEV-PC is not possible according to the data sheets. Even the 3 C charging for the HEV-B is not generally possible, but only for 5 cells. The discharge rate of 2 C for the BEV-PC is possible for all cells, whereas the charge rate of 1 C is possible for 8 out of 13 cells.

The price information is based on manufacturers' information for large quantities. Only few companies provided this information. The targeted battery cost is between $200 and $300/kW h according to the U.S. Advanced Battery Consortium, the Sloan Automotive Laboratory at MIT and the Electric Power Research Institute, all in the United States [5]. This is the cost for a complete system. The table shows that this seems not attainable with the nowadays cell prices, except maybe for cell H.

3. Enhanced test methodology

Although some cell tests methods are described in the scientific literature [6–12], as a rule one uses individual test schemes to evaluate the performance of batteries. Unfortunately, these are not based on the international standards that are under development [13]. In this article the main international battery test standards are applied, i.e. [2,14–18]:

- IEC 62660-1 (performance testing for lithium-ion cells)
- ISO/DIS 12405-1 (lithium batteries for vehicles, high power applications)
- draft ISO/DIS 12405-2 (lithium batteries for vehicles, high energy application)
- IEC 61982-4 (battery test for BEV)
- FreedomCAR battery test manual (battery tests for HEV)
- DOE battery test manual for plug-in hybrid electric vehicles (tests for PHEV)

The test standards are all for lithium-ion batteries except IEC 61982-4 that can be used for all automotive batteries.

A couple of test methods are found in most of the standards:

- Capacity tests consisting of full discharges and recharges of a battery.
- Pulse tests containing a pulse train consisting of a combination of a discharge and charge pulse, sometimes at several C-rates. The pulses can also be expressed in kW in the FreedomCAR manual and DOE battery test manual.
- Cranking test at low and possibly high temperature.
- Self discharge test.

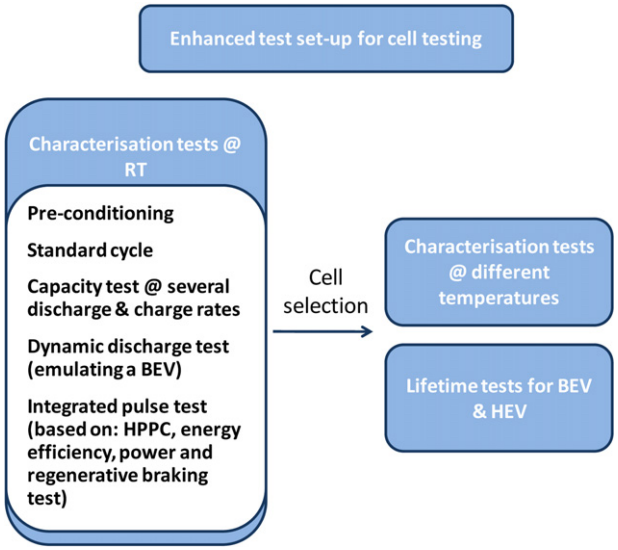

Fig. 1. Enhanced test set-up based on the 6 main (draft) standards.

The tests are often repeated at several temperatures. Notwithstanding the four test categories that can be discerned in the standards, they are always executed with dissimilar charge rates, rest periods and SOC levels. So, it is not possible to bring those tests easily together. The discussion on the test standards and how they have been combined into an enhanced test methodology to characterise cells is given in [4].

The following characterisation tests can be based on the standards, see also Fig. 1:

- Pre-conditioning in order to condition the fresh cells and being a first quality control.
- Capacity test at several discharge and charge rates: The test is performed at 6 discharge rates and equivalent charge rates if allowed, i.e. $0.33I_T$, $1I_T$, $2I_T$, $5I_T$, $10I_T$ and max. allowed I_T. I_T is the current relative cell capacity as declared by the manufacturer, not necessarily the 1 h capacity. The broad range of discharge rates reflects both the (P)HEV and BEV applications. It also allows a good comparison of the available cells given that, except the NiMH-cell, they all accept 5 C discharging and many 10 C. If the 1 C capacity that can be calculated from the measurements, appears to differ more than 5% from the one given by the manufacturer (called I_T) than the calculated 1 C value will be employed for the subsequent tests.
- Dynamic discharge test in order to obtain many cell properties like efficiency under dynamic conditions closer to reality than during capacity tests: it consists of a 4 step profile with maximum discharge rate of 1.6 C and an average discharge rate of 0.33 C. It should simulate the BEV behaviour.
- An integrated pulse test consisting of a series of 8 discharge and charge pulses that are executed at 5 SOC levels: 80, 65, 50, 35 and 20%. This is shown in Fig. 2. If the maximum allowed charge pulse is lower than the discharge pulse, the charge duration is increased proportionately to maintain the same SOC level, the so-called charge sustaining operation. In this way the efficiency of the discharge and charge pulse combination can still be calculated.

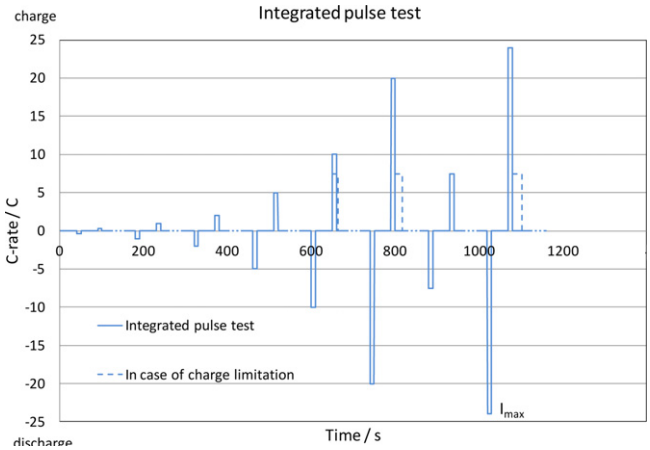

Fig. 2. Integrated pulse test consisting of 8 pulses [4]. The pulse period is 10 s or increased in case of charge limitation (charge sustaining operation). The time between a discharge and charge pulse is 40 s and the interval after a charge pulse is 10 min.

The tests are first performed at room temperature and a selection of the cells will be subjected to tests at other temperatures (Fig. 1). Each test will be executed with 5 samples of each cell. This enables data on the repeatability of the tests and the variation between the samples. In the next paragraphs, a detailed description is provided of the individual test results.

4. Main battery materials for automotive Li-ion cells

The material that designates the name of a Li-ion battery cell is often the cathode material. This is since the anode material is classically carbon-based (graphite or coke) although new materials (lithium metal alloys, metal based alloys, C composites and lithium titanium oxide) are coming to the market. Four basic cathode materials are used in the commercial batteries [19–21]:

- $LiCoO_2$ (LCO)
- $LiNiO_2$ (LNO)
- $LiMn_2O_4$ (LMO)
- $LiFePO_4$ (LFP)

LCO was the first one being used and has a high capacity. That is why it is found in most consumer type batteries, but Cobalt is also the most expensive metal in the mentioned cathode materials. It has a layered crystal structure. LNO possesses the best capacity and power. However, the layered crystalline structure is not stable, decreasing the lifetime [22]. The thermal stability is low as well. The manganese oxide is known for its stability due to a different (spinel) crystal structure that is more stable and has no or little excess lithium ions in the fully charged state. This provides very little lithium ions for undesirable lithium metal deposition on the negative electrode in overcharge. Also, the threshold of thermal decomposition of the charged (lithium-depleted) material is at a considerably higher temperature than that of the previous materials. However, at above-ambient temperatures it dissolves in the electrolyte. This can be reduced by adding foreign ions and an oxide coating [23].

For automotive batteries on the market, mixtures of the first three materials are used, leading to [19–21,24]:

- $LiNi_{0.85}Co_{0.1}Al_{0.05}O_2$ or NCA
- $LiNi_xCo_yMn_zO_2$ or NMC

NCA approaches the favourable power and capacity characteristics of $LiNiO_2$ and is cheaper than $LiCoO_2$. The addition of Aluminium suppresses a phase change in the crystalline structure that is dependent on the Li-concentration and minimises volume change. Saft and Toyota have demonstrated long life of NCA (15 years, 350,000 charge cycles) [24]. These properties make NCA attractive for electric vehicles. Disadvantages include safety concerns and cost. NCA cathodes are the most thermally unstable of the automotive Li-ion chemistries and they begin to degrade at high charge levels (high charge increases the chances of thermal runaway, which may mean that these batteries cannot use all of their capacity) but also at low charge levels due to a change in crystal shape. They are still expensive due to heavy use of cobalt and nickel. Safety and life expectancy concerns have been resolved through engineering, i.e. separators, cooling systems and controls to prevent over-discharge and overcharge.

Safety and cost concerns on NCA have resulted in the development of NMC. Various compositions are possible, combining the capacity of $LiCoO_2$, safety of $LiMnO_2$ and both capacity and power of $LiNiO_2$. The 1-1-1 ratio or $LiNi_{1/3}Co_{1/3}Mn_{1/3}O_2$, seems to be the most popular composition. The nickel also stabilises the crystal structure in discharged state, improving the cycle life. This chemistry helps reduce costs and is believed to be safer, but cycle life at high charging (oxidation and gassing occur, impedance rises at high charge), safety, and cost remain a challenge.

Some companies promote the use of $LiMn_2O_4$ but in combination with a distinct anode: lithium titanate oxide (LMO + LTO). In the contrary with the usual graphite anodes, it does not react adversely with the commonly used electrolytes in Li-ion cells, hence no passivation (SEI) layer is formed. The resultant batteries become more stable, charge quickly, even at low temperatures, they are long lived, and a wider range of their capacity can be used (i.e. 0–100% charge). The disadvantages are that lithium titanate batteries contain less energy since they operate nominally at approximately 2.5 V instead of around 3.6 V for the earlier mentioned chemistries, which may require automakers to use more cells of them. They are expected to be more expensive than NMC batteries. Appropriate applications for this technology include those that require ultra long life, low energy, but high power applications such as in HEVs [24].

Lithiated iron phosphate (olivine crystal structure), denoted LFP, is the newest cathode material of the listed four and uses cheaper materials than the previous cathodes. It is not a metal oxide but belongs to the polyanions. Since its lower electrochemical potential in comparison to NCA and NCM, LFP is less likely to oxidise the electrolyte solvent and thus is more stable, especially at elevated temperatures. It has a nominal potential of approximately 3.2 V. Originally, the electron conductivity was not good, but breakthroughs removed this item, i.e. coating the particles with carbon, making it easier for electrons to move through the material [25] and doping the material to adapt its electronic structure [26,27].

LFP cathodes have the highest thermal decomposition temperature combined with the lowest energy release, making them intrinsically safer and they are more resistant against overcharging than the previous materials. On the negative side, LFP batteries appear to have weaker cold weather performance, and they may be more challenging to monitor electronically given an almost flat potential curve as function of the state of charge. The flat curve is a result of a phase change that occurs in the material during (dis)charge keeping the potential almost constant [28]. Their volumetric energy density is lower than for NMC materials, which can be a drawback for use in EVs.

Not only the chemical composition of the materials play an important role, but also the shape of the particles and their surface morphology. These aspects can improve the Li-ion transport and minimise cracking [29]. Small particles

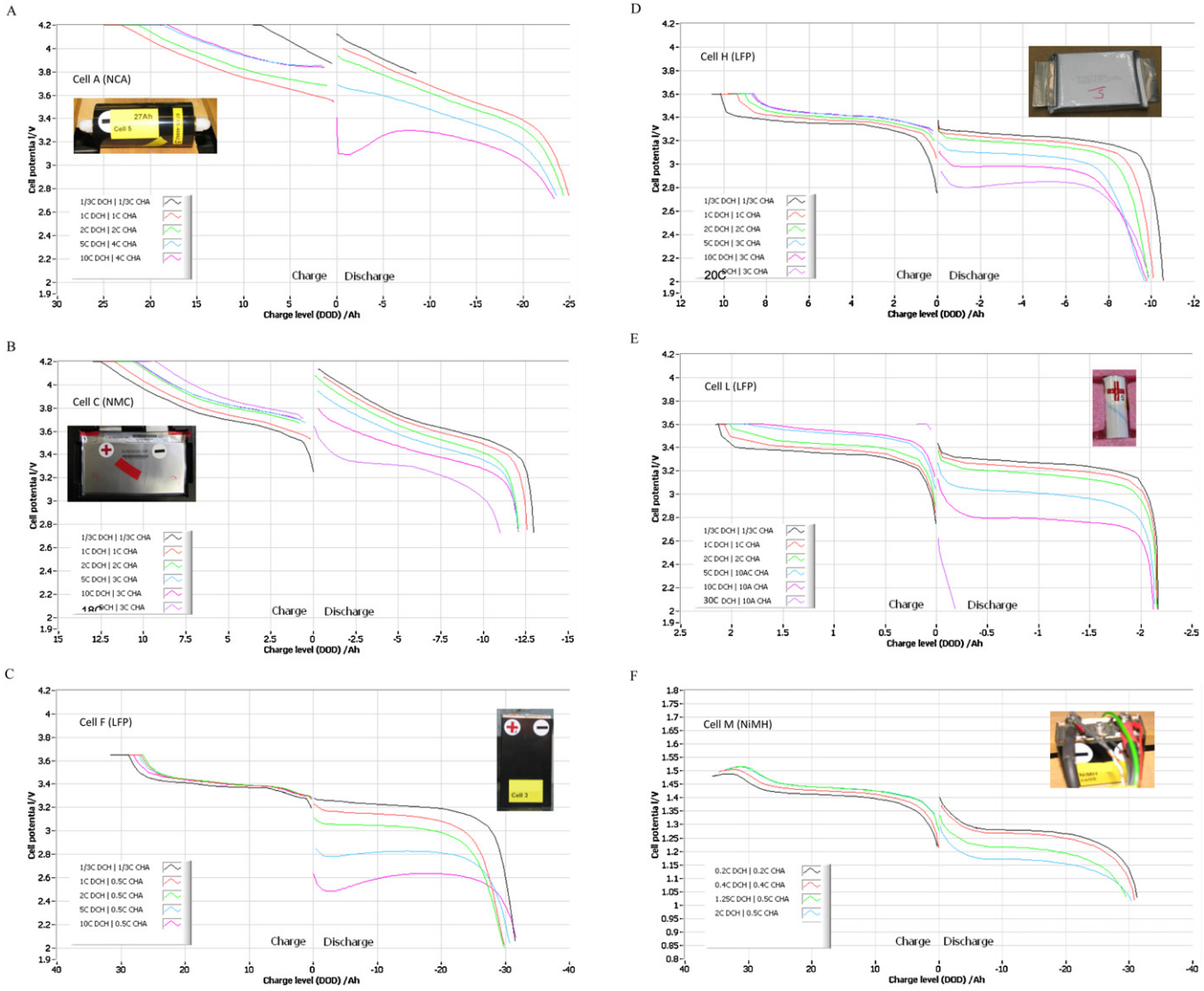

Fig. 3. (Dis)charge cell potential against (dis)charge level (A h) at distinctive (dis)charge rates for 6 cells. (A) Cell A (NCA), the 1/3 C curve is very short due to a programmation error: the maximum (dis)charge time was accidentally fixed to 1 h; (B) cell C (NMC); (C) cell F (LFP); (D) cell H (LFP); (E) cell L (LFP); (F) cell M (NiMH), the voltage drop during charging is clearly visible at the left.

are required but nano-size may lead to safety and stability items [21].

Regarding the electrolytes [30], they are mostly lithium salts in solvents. Some manufacturers use ionically conducting polymers, often mixed with ceramic nano-particles. Solid-state electrolytes, consisting of conductive crystals and ceramic glasses without a need for separators between the electrodes, exist too but are hardly incorporated in battery cells on the market.

Other important materials [21,31] are binders to improve conductivity and structural integrity of the electrode material, electrode coatings to control passivation (SEI) layer and to improve wetting, nano materials to improve current handling capability and buffering large volume changes, and additives, also called Black Magic. Numerous proprietary additives are used in the electrolyte and the electrodes to improve both electrical and thermal conductivity, reduce flammability and suppress dendrite formation.

5. Individual cell test results

The cells are tested with help of cell testers (−5 to 5 V) and battery testers (−5 to 80 V) manufactured by PEC Corporation. An interesting feature is that they consist of 50 A channels that can be put into parallel up to 600 A. In this way, more or less batteries can be tested at the same moment depending on the maximum C-rate of the test and the individual cell capacity. This assures that a maximum of cells can be tested during the test period.

5.1. Capacity test and Peukert constant

In this paragraph some characteristic (dis)charge curves are shown and discussed. A new feature is the way of presenting: discharging and charging in the same plot side by side (Fig. 3). This has been enabled by the adaptation of the test standards to charge the cells at the same rate as the discharge rate. From the capacity test also the Peukert constant can be derived by fitting the discharge time for each discharge rate with help of a power law. The exponent is the Peukert constant and the factor is the Peukert capacity. This shows the current rate dependency of the capacity. For lead-acid batteries this effect is very clear. For Li-ion batteries it is generally much less pronounced but still present [32]. The capacity test is also used to determine the actual 1 C capacity, according to:

$$1\,\text{C capacity} = (\text{Peukert capacity})^{1/\text{Peukert constant}} \quad (1)$$

Table 3
Peukert constant and capacities from capacity test.

Cell	Type	Peukert constant (–)	Peukert capacity (A h)	1 C capacity (A h)	Declared capacity (A h)
A	NCA, cylinder	1.032 ± 0.06	27.6 ± 0.5	24.9 ± 0.1	27
C	NMC, pouch	1.04 ± 0.01	13.6 ± 0.3	12.3 ± 0.3	12
F	LFP, prismatic	0.998 ± 0.04	30.5 ± 0.5	30.71 ± 0.04	30
L	LFP, cylinder	1.007 ± 0.002	2.16 ± 0.01	2.15 ± 0.01	2.3
M	NiMH, prismatic	1.024 ± 0.008	32.9 ± 0.5	30.3 ± 0.6	30

Six cells have been put together in Fig. 3 because they contain a dissimilar cathode chemistry or they show a remarkable behaviour. Fig. 3A shows the (dis)charge plot for cell A (NCA, cylinder). The discharge capacities are close to each other and diminishing with increased current rate. At the maximum current rate of $10I_T$, the potential drops quickly but recovers. This is probably due to the heating of the cell. A similar effect is observed in [33]. The 1 C capacity differs 8% with the value given by the manufacturer (27 A h at 0.2 C) as can be seen in Table 3. Therefore, the capacity (I_T) will be replaced with the 1 C capacity in the next tests.

Fig. 3B shows the result for cell C (NMC, pouch). The (dis)charge plot for cell B is almost the same, but with fewer curves due to a much lower maximum current rate. Note that the curve at maximum discharge rate ($18I_T$) is different from the others. The accompanying capacity is clearly much lower. The manufacturer may be too optimistic with this high current rate. It has not been included to determine the Peukert equation. The capacity for the other curves is close to each other and decreasing with current rate. From the measurement data the figures on Peukert constant, Peukert capacity and 1 C capacity are derived. These are given in Table 3.

Fig. 3C shows the (dis)charge plot for cell F (LFP, prismatic). It is to a large extent the same as for cell E. However, for this cell the capacity increases for the highest discharge rate of $10I_T$. Also, it is visible that for the highest discharge rate the potential drops but recovers temporarily. Both effects are most probably due to the temperature rise in the battery cells, since they heated up to $57 \pm 9\,^{\circ}C$ at the highest discharge rate. The capacity decreases at a discharge rate of 1 C and 2 C, but increases in comparison to the 2 C capacity for the discharge rate 5 C and 10 C. The latter leads to an identical capacity as for the 0.33 C discharge rate for all 5 samples. This leads to a Peukert constant being 1.

The drop in potential with subsequent recovery at high current rates as observed above, is much less visible for the tested LFP pouch cells. It is only visible for cell H, and then only at $20I_T$ (see Fig. 3D). (Cell H is the only cell for which the manufacturer allowed $20I_T$ discharge.) It is also the only LFP pouch cell that has a higher capacity at the highest C-rate. So, both effects seem to be coupled to each other.

The drop and subsequent increase in potential is not observable for the 3 kinds of LFP cylindrical cells that have been tested. Fig. 3E shows the result for cell L. The manufacturer promised a highest discharge rate of $30I_T$. However, it is an overbid. The potential drops almost instantaneously to the minimum allowed. The discharge capacity is then only one tenth of the capacity at the other rates. At the other rates, the discharge capacity is almost identical. The measured 1 C capacity (see Table 3) differs 7% with the value given by the manufacturer (2.3 A h). This is outside the 5% limit; it implies that the C-rate has to be changed for the following test procedures to 2.15 A h.

Fig. 3F shows the (dis)charge plot for cell M (NiMH, prismatic). The discharge rates have been taken as 1/5 of the ones for lithium-ion cells, resulting into 0.2, 0.4, 1 and $2I_T$. The potential drop during charging is clearly visible. The highest discharge curve shows a slight increase in capacity. The Peukert constant is close to 1 as for lithium-ion cells.

5.2. Cell potential plateau in discharge operation

The discharge profiles show a quick initial decrease in cell potential, a deflection point and subsequent a cell potential plateau with an almost linear drop in cell potential and after a second inflection point, again a quick voltage decrease when the battery cell becomes empty. At high current rates the curve between the two inflection points may not be linear, probably due to temperature effects on the cell potential as discussed in the previous paragraphs. The slope of the plateau for LFP cathodes is reported to be flat due to a phase change during discharge [33]. However, in Fig. 3C–F which show the (dis)charge curves for LFP battery cells, the slope is small but not flat. This is probably due to a potential increase in the anode material. The potential of graphite is typically between 50 and 200 mV vs. Li^+/Li depending on the specific charge capacity [34]. The cell potential drop of around 100 mV between the inflection points for the 0.33 C, 1 C and 2 C curves are in line with this.

Fergus [21] made a study on the range of cell potential plateau values as found in literature data for the cathode materials: $LiCoO_2$, $LiMn_2O_4$, $LiNi_{0.33}Co_{0.33}Mn_{0.33}O_2$ and $LiFePO_4$ for 1 C discharge rates. Those findings can be compared with the tested cells. To compensate for the anode potential vs. Li^+/Li, the ranges found in [21] have been subtracted with a single 150 mV based on the graphite potential range as given above. The result is shown in Fig. 4. It appears that the cell potential plateau ranges for the cells are in line with their chemistry. For the NCA and NMC cells the lowest value is much higher than the bottom of the reference window. This may indicate that the fabrication of the battery materials have been well optimised to enable good discharge performance. However, cell I shows a lower voltage range of approximately 0.2 V than

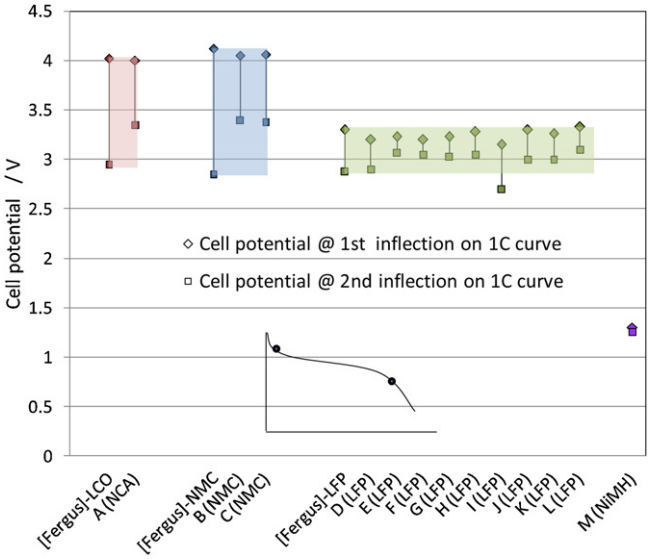

Fig. 4. Ranges of cell potential plateaus for the tested cells in comparison to values found in the literature study [21] (called Fergus on the *x*-axis, after the author). The inset shows the concept of inflection points with the cell potential plateau in-between.

found in the literature study. This may indicate a higher potential of the anode vs. Li^+/Li. For NiMH the 0.2 C discharge curve has been taken to determine the cell potential plateau range. The range appears to be very small in comparison with the Li-ion cells.

5.3. Temperature increase

Up to 5 C discharge, the cells do not need additional cooling. 5 out of 9 cells that can cope with a 10 C discharge need forced cooling by a ventilator. 2 cells out of 3 that withstand even higher discharge rates need forced cooling.

Fig. 5 shows the maximum temperature distribution at the highest allowed discharge rate for the cells dealt with in the previous section. Cell A (NCA, cylinder) becomes the hottest in the middle with 57 °C at $10I_T$. Cell C (NMC, pouch) has additional cooling. It becomes hottest at the anode side with 46 °C at $18I_T$. Rectangular stickers are attached to be sure that camera does not see reflection of the aluminium housing and in that case will underestimate the temperature. Cell F (LFP, prismatic) becomes hottest at the cable connection, specifically at the cathode side with 59 °C at $10I_T$. Cell E (not shown in the figure; it is like cell F but with higher capacity) even becomes 100 °C in that corner. The next samples of this cell have been cooled. Cell H (LFP, pouch) becomes hottest in the middle of the pouch with 62 °C at $20I_T$. The cylindrical cell L becomes 46 °C at $10I_T$. The temperature is almost uniformly distributed. The NiMH prismatic cell (M) becomes warmest in the centre with 44 °C at $2I_T$.

From the thermo-graphical pictures it is clear that the cells react differently under load, even if the same cell shape is compared. The central part can be hottest but also the anode or the cathode.

5.4. Dynamic discharge pulse test and integrated pulse test

Fig. 6 shows a small part of the dynamic discharge pulse test. Since it reflects a battery electric vehicle behaviour, it is of interest to include results from this test in Table 4 . This table shows a concise overview of the test results and makes it more easy possible to compare the individual cell results, what will be performed in the next section. The DDP-capacity, its efficiency and the average cell potential is included.

Fig. 7 shows the integrated pulse test executed on cell L. It is clear that a pulse train of 8 discharge and charge pulses are performed at 5 SOC levels. The 8 pulses allow to find the efficiencies of small pulses up to large pulses and also to compare cells given that not all cells can withstand the same maximum C-rate. Testing with a series of pulses permits that there is always a pulse strength that also has been tested for other cells. This enables the comparison of the cells. The pulse at maximum pulse current for cell L (52 C pulse) leads to an instantaneous voltage collapse. Zooming into the 20 C pulse train, as shown in the figure, shows that the charge pulse (4 C) has been prolonged in order to enable a charge equilibrium between the discharge and charge pulse as prescribed in the test procedure. This is reflected in the cell potential that reaches the same level as before starting the 20 C discharge pulse.

6. Comparison between cells

This section presents a summary of the individual test results in table form. The results are discussed and afterwards a selection is made for cells that seems of most interest for the intended 4 automotive applications (see Section 2). Six cell properties are visualised in function of the cathode chemistry and cell shape (Fig. 8). Also 3 supposed physical relationships are represented in Fig. 9.

6.1. Structure of the cell property table

Table 4 shows a concise overview of the cell properties. It starts with manufacturer data like cell chemistry, shape and declared (dis)charge rates. The second part shows test results on capacity, efficiency and temperature at two discharge rates, i.e. $1I_T$ and $5I_T$. These have been selected since 1 C is a standard reference and 5 C can be performed by all cells except the NiMH, offering the best comparability. The third section shows other interesting parameters like the internal resistance and energy density. The fourth section shows the pulse power densities and accompanying efficiencies.

In the table, cells have been classified by colour for important properties regarding (PH)EV vehicles. The properties that are esteemed as important are explained below. In green are the best performing cells, in yellow the second best and in red the worst ones. If values are in blue, it means that the cells do not perform as the manufacturer indicates.

6.2. Capacity, discharge and charge rates

Table 4 (section 1) shows that three types of lithium-ion chemistries (regarding the cathodes) are amongst the cells. Most of the cells are $LiFePO_4$ cells (LFP). The capacity of the cells ranges from 2 A h up to 70 A h. Quite a large difference exists in terms of (continuous) discharge rate with rates between 6 and 20 (leaving aside the 30 C that is not achievable). The '„' sign indicates that the peak rate is identical to the continuous rate since no specific information is given by the manufacturer. The NiMH cell has a lower discharge rate what is due to the different chemistry. So, it is not comparable with the lithium-ion cells. The continuous charge rates are modest with values between 0.5 and 4 C. The peak charge rates are hardly higher, at least since most of the manufacturers do not give information on this in the datasheets. For three cells (A, D and L) the capacity is lower than officially designated. One cell (L) does not achieve the assigned discharge rate in continuous discharge and in peak discharge. This shows itself in a very reduced capacity, being only a fraction of the 1 C capacity due to a quick voltage drop to minimum allowed level as can be seen in Fig. 3E.

6.3. Efficiency and temperature behaviour

Table 4 (section 2) shows that all cells behave well, achieving efficiencies of 74–96%, also at 5 C discharge rate (without external cooling). The efficiency that is found with the dynamic discharge power (DDP) test for BEV cars is close to the 1 C efficiency. Also the DDP capacity is close to the 1 C capacity. The lowest efficiency is observed for the NiMH cell. This efficiency is still good for such a battery type since in [35] a range is given from 50% for conventional NiMH cells up to 85% for the most modern ones. However, if it is used in a 50% DOD range omitting a complete charge that heats up the cell [36], then the efficiency (1 C) increases to 90% according to additional measurements. The energy density consequently halves from the already low 44 W h/kg to 22 W h/kg. The 5 C efficiencies are graphically shown in Fig. 8A with the cell description as *x*-axis. From the graph can be observed that it seems that the efficiencies for NMC are slightly higher than for the other cells. Also the pouch cells behave better than average. The prismatic shape seems to have a clear negative effect on the efficiency. The spread in efficiencies shows that it is influenced by many design factors.

The heating of the cells during discharge is very different amongst the cells. At a 5 C discharge rate (this rate is attainable for all cells except the NiMH one) the temperature is between 29 and 52 °C (without additional cooling for all cells). It is graphically shown in Fig. 8B with the cell capacity as *x*-axis. The heating behaviour cannot be contributed to the cathode chemistry and cell

Table 4
Main results from the characterisation tests. The values are the average for 5 samples of a cell given together with the standard deviation („ indicates identical to previous value of the same property).

ID		A	B	C	D	E	F	G	H	I	J	K	L	M
Cathode		NCA	NMC	NMC	LFP	LFP	LFP	LFP	LFP	LFP	LFP	LFP	LFP	NiMH
Shape		Cylinder	Pouch	Pouch	Prismatic	Pouch	Prismatic	Pouch	Pouch	Cylinder	Cylinder	Cylinder	Cylinder	Prismatic
Connection		Screw	Flap	Flap	Screw	Flap	Screw	Flap	Flap	Screw	Side	Side	Side	Screw
Nom. Cap.	Ah	27	70	12	45	40	30	14	10	10	3.5	2.5	2.3	30
Discharge rate	C (cont.)	10	5	18	10	10	10	10	20	8	10	6	30	2
	C (peak)	„	8	23	„	„	8	20	40	„	„	20	52	„
Charge rate	C (cont.)	4	2	3	0.5	2	0.5	0.5	3	3	2	0.5	4	0.5
Charge rate	C (peak)	6	3	„	„	„	3	1	6	„	„	1	„	„
1C Capacity	Ah	24.9	71.8	12.3	39.8	39	30.71	14.22	10.1	9.6	3.6	2.43	2.15	30.3
(Peukert fit)	±Ah	0.1	0.4	0.3	0.5	1	0.04	0.04	0.2	0.3	0.1	0.03	0.01	0.6
DDP-capacity	Ah	24.3	73.1	12.2	39.6	39	31.5	13.94	10.4	9.8	3.6	2.51	2.121	30.0
	±Ah	0.2	0.3	0.1	0.6	1	0.5	0.01	0.2	0.3	0.1	0.04	0.006	0.7
DDP efficiency	%	93.2	94.3	95.9	84.2	91	87.9	92.8	93.3	88.6	93.0	92	94.4	74
	±%	0.2	0.1	0.1	0.7	4	0.9	0.1	0.5	0.6	0.3	1	0.2	1
Eff. @1 C	%	93.1	93.6	95.1	89.1	92.5	87.9	92.7	92.3	87.1	89.8	90.8	94.8	74 (90)
	± %	0.1	0.3	0.4	0.5	0.2	0.9	0.2	0.3	0.3	0.3	0.6	0.1	4
Eff. @5 C	%	84.6	87.1	90	80	85	80.4	86.6	85.6	75	80.5	82.8	84.7	N.A.
	± %	0.4	0.3	1	1	1	2.6	0.2	0.6	1	0.6	0.9	0.6	
Temp. @5 C	°C	38	39.2	31	52	39.4	51	39	36	46	33	36	29	N.A.
(no cooling)	±°C	7	0.8	5	1	2.6	4	2	1.2	2	7	3	2	
Temp. @Imax	°C	48	–	38	48	33 / 52	57.0	39	52	57	31	40	24	34
	±°C	10	–	7	9	3	9	4	3	3	6	2	2	1
Cooling @Imax				YES	2,3,4,5	1,2,3		Yes			Yes		Yes	
SOC @CV, 1C	%	92.0	88.5	92.1	91.8	92.0	87.9	98.3	92.6	84.3	81	85	96.5	N.A.
	± –	0.1	0.4	0.7	0.6	0.9	0.9	0.1	0.2	0.7	1	3	0.2	N.A.
Peukert coeff.	–	−1.032	−1.029	−1.04	−1.028	−1.016	*−0.998*	−1.009	−1.014	−1.012	−1.012	−1.031	−1.007	−1.024
	± –	0.006	0.004	0.01	0.004	0.006	0.004	0.001	0.005	0.002	0.003	0.003	0.002	0.008
Internal resist.	mΩ	2.6	1.0	6	2.2	1.4	3.2	4.7	3.8	8.9	20	29	25	2.5
(1C-2C, 80% SOC)	±mΩ	0.9	0.2	2	0.2	0.3	0.9	0.1	0.6	0.6	1	3	2	0.6
AC resistance	mΩ	0.4	0.3	1.1	0.9	1.5	0.9	1.4	1.2	4	10	15	7.5	0.6
(1kHz)	±mΩ	0.2	0.1	0.1	0.1	1.6	0.1	0.1	0.5	1	1	5	0.5	0.1
Ratio DC-AC res.	–	6	3	6	3	1	4	3.4	3	2	2	2	3	4

Table 4 (*Continued*)

	± –	4	1	3	1	1	2	0.3	2	1	0	1	0	1
Energy density	Wh/kg	90	149	126	77	94	90	118	110	84	84	97	98	44 (22)
(from DDP test)	±Wh/kg	3	9	6	6	6	10	3	6	4	5	8	7	1
Average voltage	V	3.627	3.671	3.660	3.125	3.14	3.13	3.204	3.163	3.148	3.172	3.178	3.234	1.262
(from DDP test)	±V	0.003	0.003	0.001	0.006	0.072	0.011	0.002	0.004	0.003	0.006	0.009	0.002	0.002
Power density	W/kg	780	1000	1800	330	640	700	1720	3100	520	660	800	1500	80
@ 50% SOC, Imax	±W/kg	30	100	100	50	50	200	70	200	60	50	100	100	10
and @ C-rate	C	10	8	23	5	10	10	20	40	8	10	10	20	2
Pulse efficiency	%	80.5	81	78.2	74	82	74	69.7	68	72	79	80	77	87
@ 50% SOC, Imax	±%	0.5	2	0.8	3	3	4	0.3	5	4	1	2	1	3
Power density	W/kg	780	–	1070	–	640	700	1000	990	–	660	800	870	–
@ 50% SOC, 10C	±W/kg	30		60		50	200	40	70		50	100	60	
Pulse efficiency	%	80.5	–	88	–	82	74	81	86	–	79	80	86	–
@ 50% SOC, 10C	±%	0.5		0.4		3	4	0.3	2		1	2	1	

Colour codes: Best result | Second best result | Worst result | Different from specification

capacity. The prismatic shape reveals a clear influence on the temperature: these cells become the hottest. Cell L becomes clearly less warm than the other cells. The cell efficiency should have a logic inverse influence on the temperature. This is assumption is checked in Fig. 9A. This seems true, but there is clearly a large spread. Cylinder cells warm up less, especially cells J and L, and prismatic cells heat up more than expected based on efficiency alone, specifically cells D and F. The temperature and efficiency behaviour will be analysed further after discussing the internal resistance.

6.4. Charging behaviour

Table 4 (Section 3) shows that quite a large spread exists in the SOC at the moment that the maximum allowed voltage is attained (from that moment on constant voltage charging is applied). This is graphically shown in Fig. 8C. NiMH cells have no limitation of a maximum voltage, so they can be charged to 100% without reducing the current. The Li-ion cells are 81% full, up to 98%! In the latter case, the time to spend constant voltage charging is hardly necessary. No relation with cathode chemistry nor cell shape seems to exist. However, cell G and L are clearly outperforming the other cells. This must be due to optimisation of particle sizes and additional (nano-)materials to improve the current handling. This is an interesting outcome that is of importance for electric vehicles. The charge behaviour is undervalued in the test standards, already for applying several charge rates but also on identifying the transition to constant voltage charging.

6.5. Resistance

The internal resistance is shown in Fig. 8D. According to the table a large difference seems to exist between the cells, covering 1 to 25 mΩ. However, if the resistance is displayed against cell capacity it appears that the resistance is clearly inversely proportional to the cell capacity with high accuracy. Only cells H and I deviates clearly from the fit, the first one having a resistance lower and the second one higher than the trend. Also cell F has a relatively high resistance. The indicator resistance × capacity is shown on the secondary *y*-axis. It is clear that the resistance is not specifically biased by shape or chemistry.

For the AC resistance the same phenomenon exists, see Fig. 8E. This resistance has been measured by a HIOKI micro-Ohm meter on fully charged cells. The spread around the fit is a bit higher with cells H and I again being most deviating. Cells A and C have a resistance lower than the trend whereas cell E has a higher resistance, but with a large variation between cells. The indicator resistance × capacity is shown on the secondary *y*-axis. For the AC resistance it can also be inferred that no bias by shape or chemistry exists. In the third table section also the DC–AC resistance ratio is given. It reflects how the cell is built. A factor 1 indicates that ohmic losses are dominant over electron transfer and diffusion losses. A factor 6 reflects that ohmic drops are relatively low. This could be due to having much current collectors. From the standard deviation it is noticeable that the ratio is sensitive to measurement precision.

The resistance has a direct influence on the efficiency and cell temperature. The ohmic heating is far more important than the reaction enthalpies and contributes accordingly most to the cell temperature [37]. The following relation can be deduced ignoring (convection) heat loss and the reaction enthalpy:

$$\begin{aligned} &\text{Loss} = \text{heat} \\ &\text{Loss} = U \cdot I \cdot t = R \cdot I \cdot I \cdot t = R \cdot I \cdot \text{cap.} = R \cdot C_{\text{rate}} \cdot \text{cap.}^2 \\ &\text{Heat} = m \cdot c_{\text{p}} \cdot \Delta T \sim \text{cap.} \cdot \Delta T \\ &\Delta T \sim R \cdot C_{\text{rate}} \cdot \text{cap.} \end{aligned} \tag{2}$$

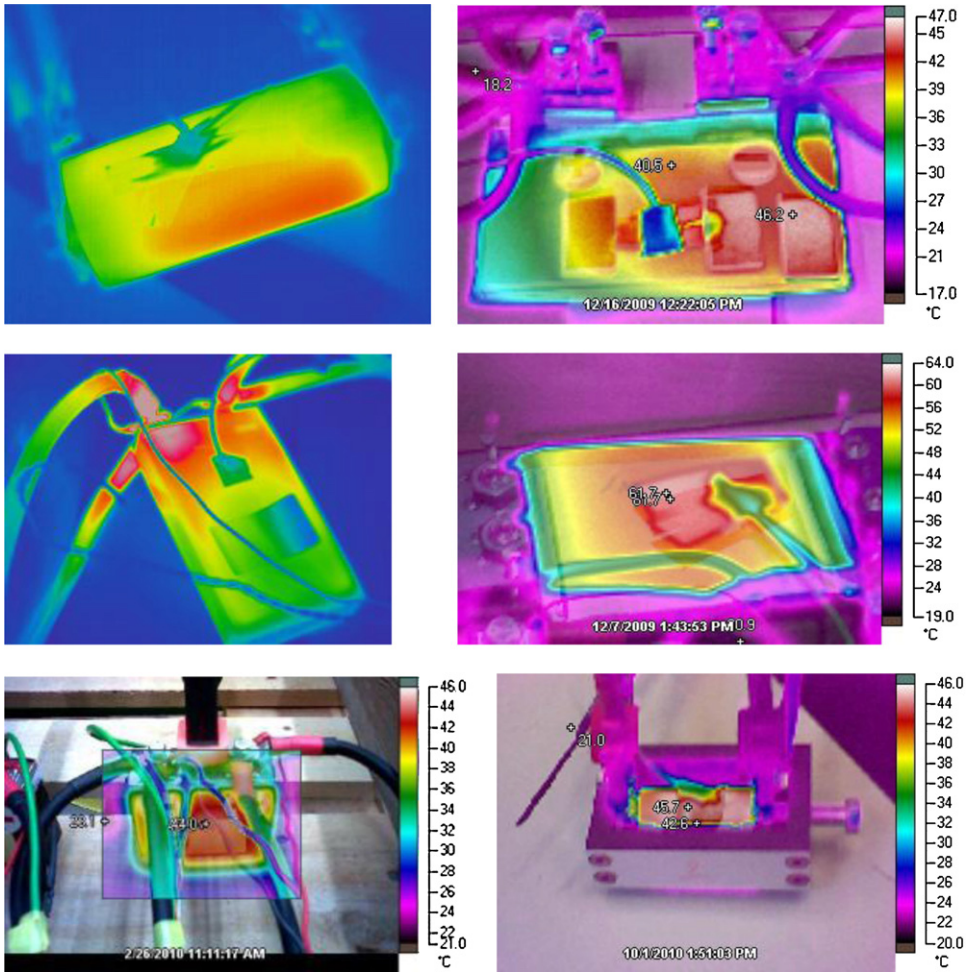

Fig. 5. Thermal photos at the highest discharge rate of cells A, C, F, H, L and M. Three types of cameras have been used, resulting in different representations.

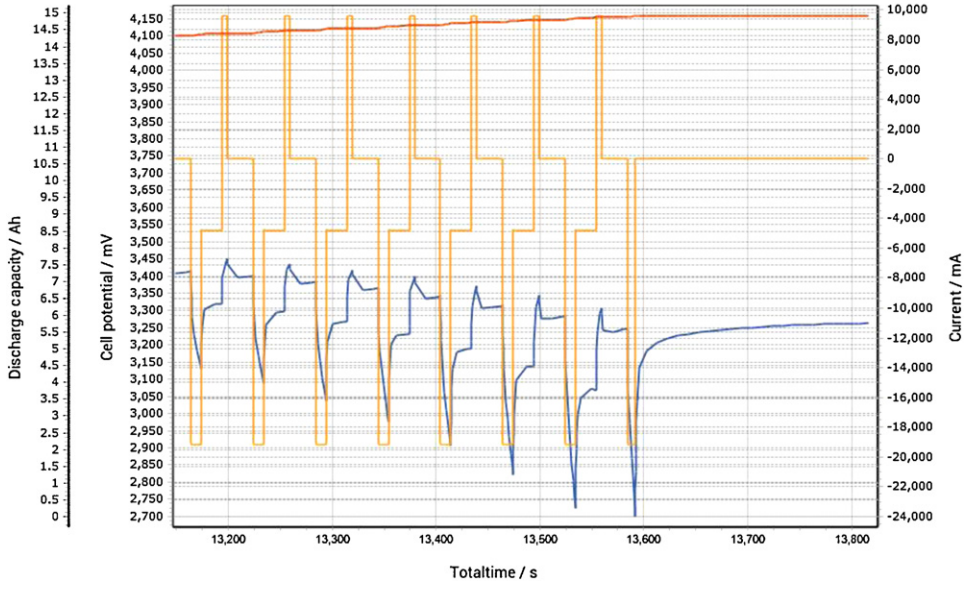

Fig. 6. The last cycles of a dynamic discharge pulse test with cell C until the cell attains the lowest allowable cell potential.

If the C-rate is equal for all cells the relation reduces to the indicator $R \times$ cap. To include the NiMH cell the C-rate has been retained and the result is given in Fig. 9B. The relation is clearly visible. Still an influence of the cell capacity appears to be visible: the small cylinder cells (J, K, L) are below the diagonal and the large cells (D, E) are above. Keeping this in mind, the NMC cells heat less than the trend. Cell H (10 A h) is an exception above the diagonal. The results for the NiMH cells seems

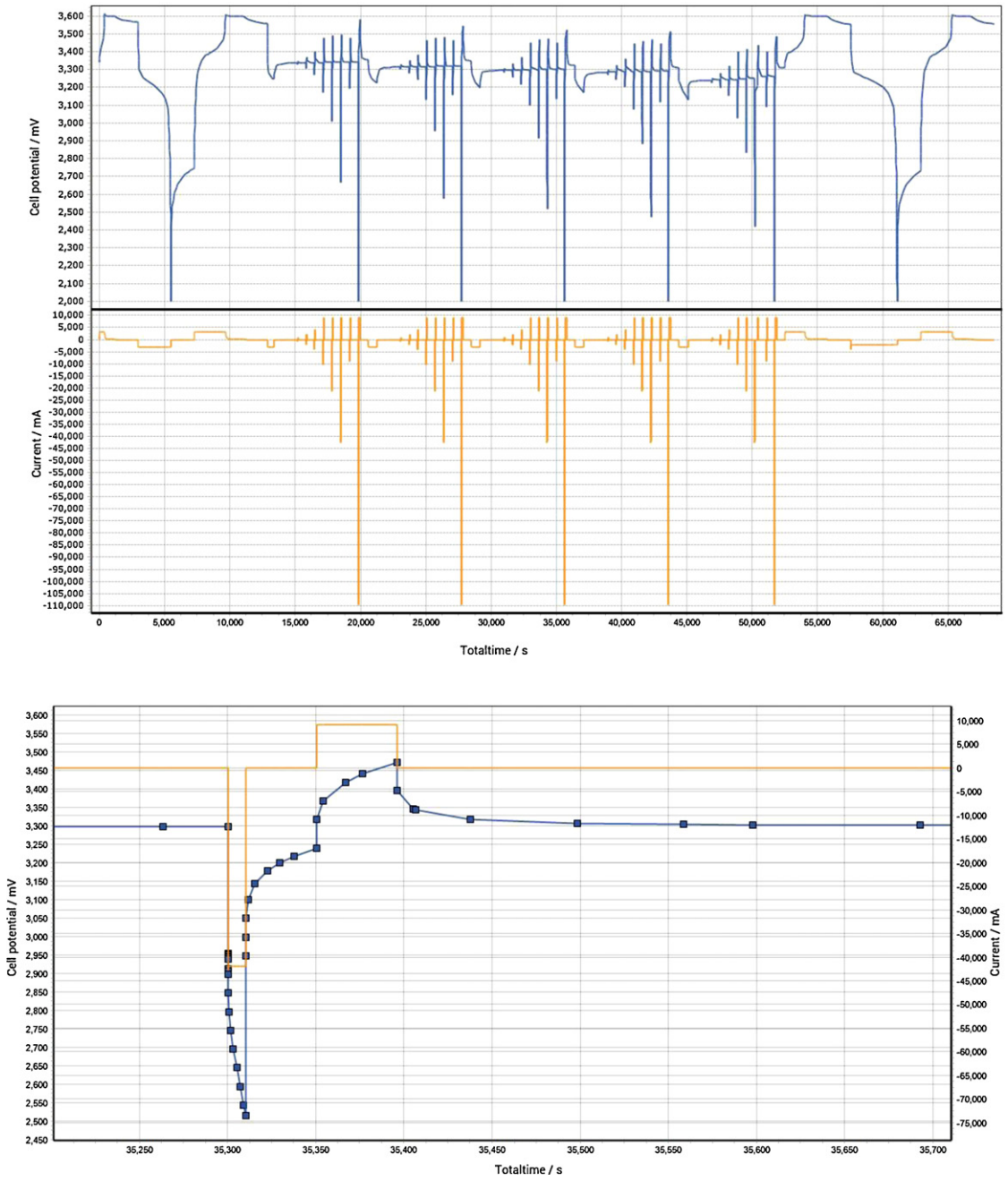

Fig. 7. Integrated pulse test performed on cell L: The complete test is shown above consisting of a standard cycle (1 C), the pulse trains at 5 SOC levels and a standard cycle. Below the 20 C pulse train at 50% SOC is shown in detail.

to follow the trend, both for cycling at 50% DOD and for full cycles.

For loss in efficiency a similar relation can be deduced:

$$\begin{aligned} \text{Ineff.} &= \frac{\text{loss}}{\text{total energy}} \\ \text{Loss} &= R \cdot C_{\text{rate}} \cdot \text{cap.}^2 \\ \text{Total energy} &= \text{cap.} \cdot V_{\text{avg}} \\ \text{Ineff.} &= R \cdot C_{\text{rate}} \cdot \frac{\text{cap.}}{V_{\text{avg}}} \end{aligned} \tag{3}$$

If the C-rate is identical for the cells and the average cell potential also, then the relationship reduces to the indicator $R \times \text{cap.}$ To include NiMH cells the C-rate and cell potential are necessary. The latter is also the case if cells with a LTO-anode are tested. The result is visualised in Fig. 9C. The relationship is quite clear. If only the indicator $R \times \text{cap.}$ is used as x-axis, then the graph would have been almost identical for these cells. The cell potential has a small influence on the location of the points of NCA, NMC and LFP cells. The NiMH cell that fully cycles does not follow the trend at all. The efficiency loss is much higher. This reveals the side reactions that occur during charging at high SOC level, mainly due to hydrogen formation and absorption [37]. Cell F is performing better than the trend. The NMC cells also have lower efficiency loss than the trend. Cell H is doing worse in Fig. 9B and C than the absolute value of efficiency and temperature make likely.

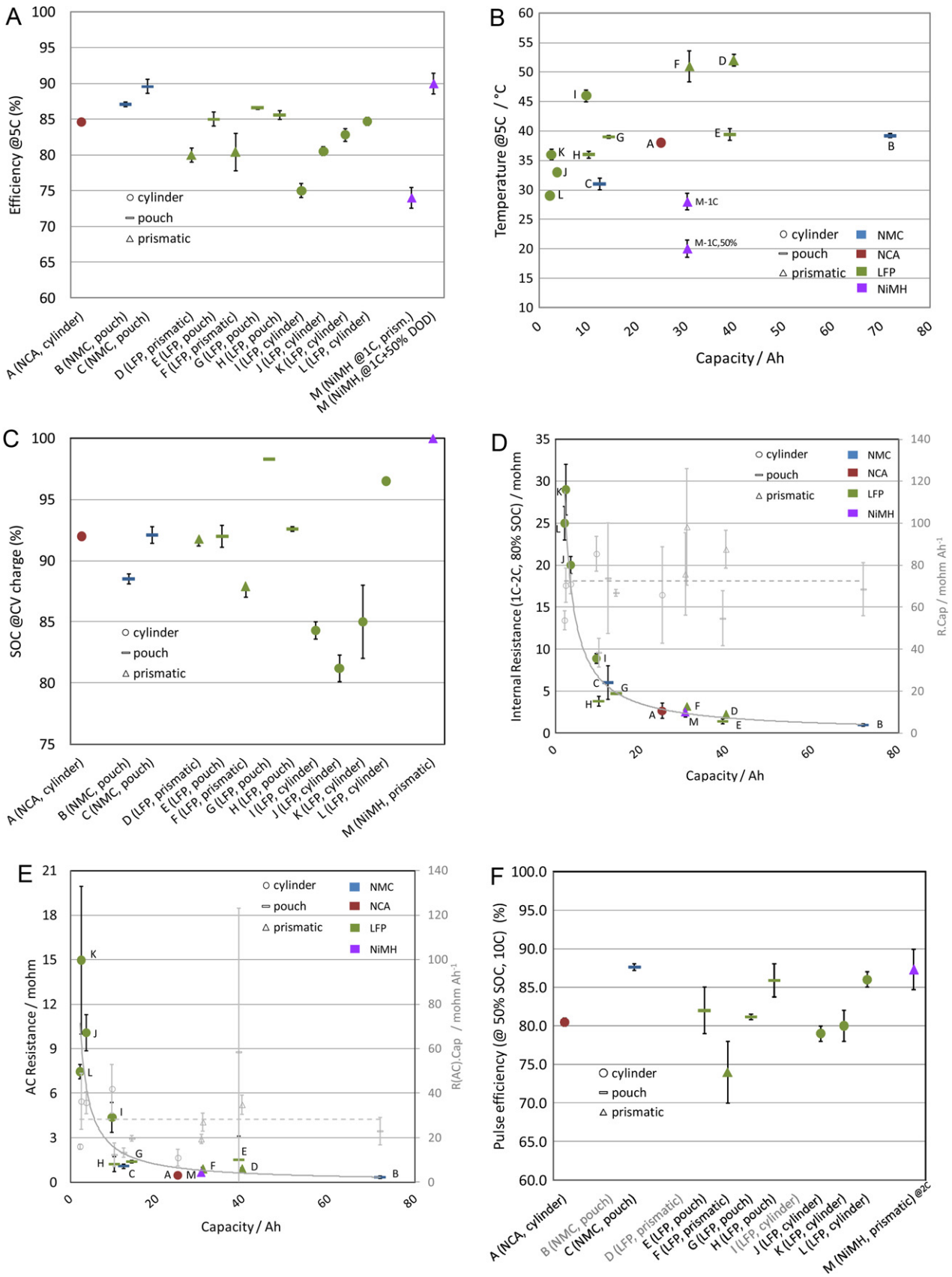

Fig. 8. Representation of test results differentiated to chemistry and cell shape. (A) 5 C efficiency, (B) cell temperature at 5 C discharge (without cooling) represented against cell capacity, (C) SOC level when attaining constant voltage charging, (D) internal resistance represented against cell capacity with the indicator $R \times$ cap. on the secondary y-axis, (E) AC resistance represented against cell capacity also with the indicator on the y-axis, (F) 10 C pulse efficiency. The discharge rates for the NiMH cell is 1/5th of the Li-ion cells.

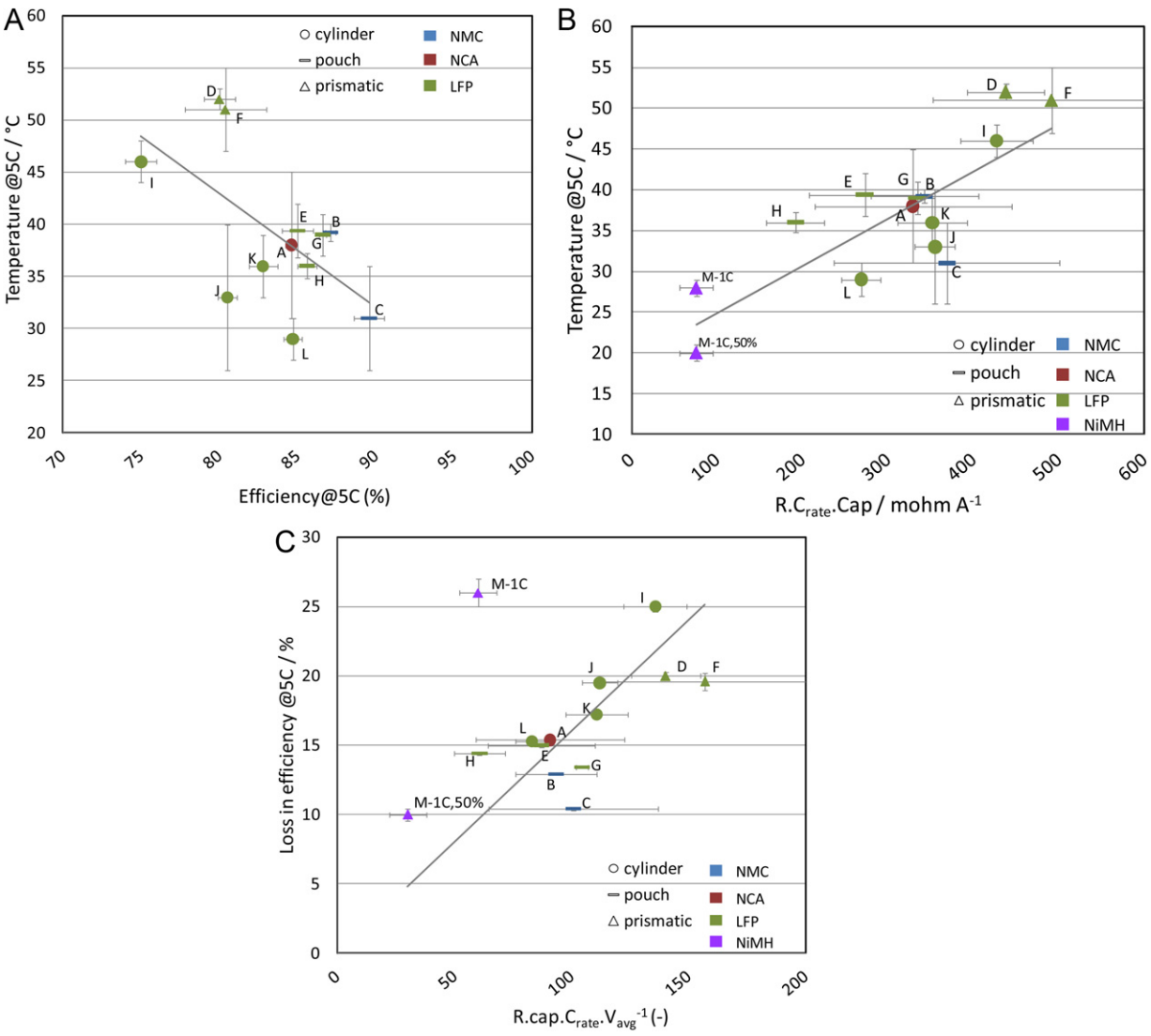

Fig. 9. Supposed physical relationships behind the test results for 5 C efficiency and temperature behaviour. (A) Temperature at 5 C discharge against corresponding efficiency, (B) the same temperature represented according to a physical relationship with resistance, C-rate and capacity, (C) loss in efficiency (100%-efficiency) according to a physical relationship with resistance, C-rate, capacity and average cell potential.

6.6. Power and energy density

Concerning the energy density, a factor 3 is discernible in the obtained values. The pouch cells perform the best, although this is not consistently the case. Most of the cells have an energy density of 100 W h/kg and only one of 150 W h/kg. That is a NMC cell. These figures are in line with the density range for nowadays cells as given in [23]. From [5] the energy density objectives on system level can be calculated from the battery objectives by the U.S. Advanced Battery Consortium, the Sloan Automotive Laboratory at MIT and the Electric Power Research Institute. These situate between 38 and 142 W h/kg. The cell test results show that for the tested NiMH it is difficult to fulfil the objectives. The upper value of the objectives is even for lithium-ion cells not really attainable.

The fourth section of Table 4 shows the pulse power density twice. The first one is at maximum pulse current. This C-rate is also added in the row below the power density. A large difference exists between the values: from 80 W/kg up to 3100 W/kg. The difference is mainly due to the C-rate of the pulse. The three best cells correspond just with the highest rates of resp. 40 C, 23 C and 20 C. There is also a large spread on the individual values of about 10%. This is composed of a spread in the cell weights, 4% on average and of a spread of the pulse voltages between the 5 tested cells of a cell samples, 6% on average. A peculiar finding from the tests is that there is more spread in the pulse voltages between the tested cells of a sample than between successive SOC levels. The latter spread appears to be 3% on average. Three cell species (D, K and L) were not able to maintain the maximum pulse according to the data sheet for 10 s. The lowest allowed voltage was attained before. This appeared to be true at all applied SOC levels. For cell D this is unexpected since the capacity test has been performed at the same C-rate without problems or a large deviation of the derived cell capacity. This means that the slope of applying the target current is of importance. In the capacity test a slope of 1 s has been imposed and in the impulse test about 1 ms, as fast as the used test cell test equipment can do. Repetition of the capacity test and the pulse led to the same result. So, the large voltage drop is not due to ageing.

The power density for 10 C pulses makes the data easier mutually comparable since most of the cells are able to withstand 10 C pulses. It appears that the best three cell types (C, G, H) have a power density of 1000 W/kg. These cells are all pouch cells. Cell B has the same power density but at 8 C. 10 C is not allowed for this cell. The worst 3 cells are F, G and J. One is a cylindrical cell, the second a prismatic one and the third is, surprisingly, a pouch cell. The

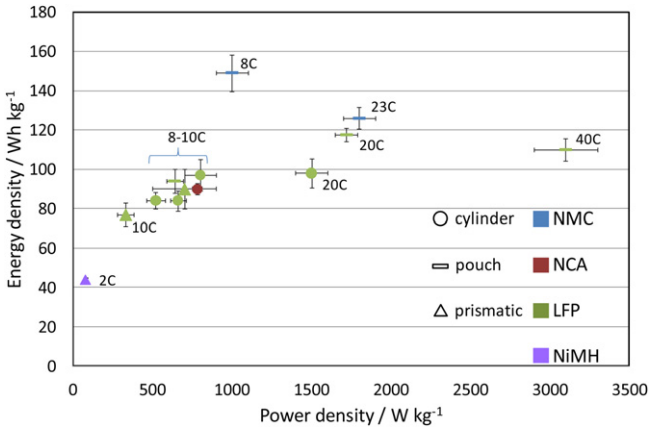

Fig. 10. Ragone-like plot of the energy density and the pulse power density.

power densities are heavily influenced by the weight of the cells that depend on the shape and the materials. So, these values cannot be related to the cathode chemistry. The pulse power efficiency for the 10 C pulses can be used to compare the cell chemistries, as depicted in Fig. 8F. The NiMH cell has been added in the figure but with a pulse rate of 2 C corresponding to 1/5th of the Li-ion pulse rate according to the reasoning that they are used in a small SOC-range [4]. It is seen that for the cells that can deliver 10 C pulses the efficiencies are all relatively close together with a band from 80 to 88%, except the prismatic cell F. So, all 3 Li-ion cathode chemistries obtain almost the same pulse efficiency values.

The pulse power density and energy density are visualised in Fig. 10 in a Ragone-like manner. Here it is clear that the tested NMC (pouch) cells have a better energy density and that some LFP cells together with one NMC cell have the best pulse power density. The similarity between the cells with highest energy and/or pulse power density is that they are pouch cells. Most of the cells perform around 700 W/kg and 90 W h/kg. The C-rate of the pulses has been added in the figure. It follows that the C-rate is determining for the pulse power density but that for an identical C-rate a spread in pulse power density is existing.

6.7. Peukert constant and cell potential

For cell selection the Peukert constant is less important as it is always close to 1. It can be concluded that LFP cells have an average cell potential of 3.2 V while NMC and NCA cells possess 0.5 V more. This may partially explain the better energy density for NMC pouch cells.

7. Discussion

7.1. Cell selection

This section discusses which cells are of most interest to test further, especially for lifetime tests. This discussion is closely related to the 4 envisaged vehicle applications.

Of most importance in Table 4 are the following properties:

- Efficiency (continuous, DDP test and pulses), since the better the efficiency, the least energy is lost.
- Heating behaviour, because it is desirable that the cells heat as less as possible in order to limit the cooling necessity.
- The state of charge when constant voltage charging commences, as during constant voltage charging the current is lower than during constant current charging, leading a longer charge time. The higher the state of charge at the end of the constant current charging, the shorter period the second charge phase needs.
- The energy density: important to know to build a small battery package.
- The power density: important to know to build a powerful battery package.

The cells with highest efficiency are cells B, C (both NMC pouch) and cell L (LFP cylinder). Cells A (NCA, cylinder), E, G, H (all LFP pouch) come at the second best place. The cells that warm up the least are cell L (LFP, cylinder), cell C (NMC, pouch), cell H (LFP, pouch) and cells J and K (LFP, cylinder).

To rank the cells, also their capacity has to be taken into consideration. Two of the four intended applications require around 30 A h cells. One application (battery electric car) needs even almost 3 times more according to Table 1. That is of course much easier realised with 30 A h cells than with 2 A h cells. In the final ranking the cells have been selected that scores best for the list as given above, with a bias for large capacity cells. The first row of Table 4 shows that four cells have been assigned as best and also four as of second interest for further testing. The NiMH cell is included here since it is the reference for HEV.

7.2. Improvements

In [4] a discussion is given on using the integrated pulse test procedure to obtain a battery model. The measurement data of the integrated pulse test can be used to fit with the FreedomCAR model [38]. This aspect has not been discussed in the above analysis. For the cell selection it was of minor importance. However, it is of importance to build a battery package and to understand its behaviour. The model appears to be of good predicting value, unless the battery package is above 80% state of charge. Still, this area is for plug-in hybrid and battery electric vehicles of interest since they are charged until full and also discharged from 100% SOC. From the measurement results, it appears that half of the number of species accept constant current charging between 92 and 98%. Also for regenerative braking it is important to model above 80% SOC. To be able to better model this area and to be able to forecast well the open circuit voltage when the battery is fully charged, the integrated pulse test has to be extended with discharge and charge pulses at 100, 95 and 90% SOC. The charge pulses should then be extended by constant voltage charging to remain at the same SOC level after each discharge and charge pulse combination, the so-called charge sustaining operation.

The slope of applying an intended current appears to be important at high C-rate. This has been repeatedly observed for the samples of one cell that was able to perform a continuous discharge at 20 C with an initial slope of 1 s to reach the 20 C current, but not able to perform a 20 C discharge pulse that was imposed in around 1 ms. The slope of imposing a current is neglected in the test standards [4].

8. Conclusions

In order to compare cells by a test methodology, an enhanced test set-up has been created based on 6 existing test standards. A wide variety of 13 cells were tested, consisting of 3 lithium-ion families and 1 nickel-metal hydride cell, and with capacities ranging from 2 A h up to 70 A h.

The underlying standards “as is” do not allow a straightforward comparison of commercial battery cells, as they were developed for specific applications on battery level, such as power assist for a hybrid electric vehicle, and the battery manufacturer has to decide how many cells (and modules) are needed. The adaptation into an

enhanced test methodology has opened the possibility of a scrutinous comparison of cell properties.

The test results have been presented in a table in a way that the cells are maximally comparable. This has been done in more depth than available in the literature before, including the spread between 5 species of the same cell. Their tests results have been systematically compared to the material properties and cell shape with help of 11 graphs arranged in 4 figures (Figs. 4, 8, 9 and 10).

All cells behaved well under the characterisation tests at room temperature. Nevertheless the differences in the individual properties like the efficiency and heating behaviour at a specific C-rate are large. The upper value of the energy density objectives as proposed by some American institutes and the U.S. Advanced Battery Consortium, i.e. 142 W h/kg, seems hard to reach. From the integrated pulse tests it is observed that there is more spread in the pulse voltages between the tested cells of a sample than between successive SOC levels.

Clear relations to cell (cathode) chemistry can be found for cell potential curves (Fig. 3), cell potential range (Fig. 4), and energy density (Fig. 10). The influence of cell shape and chemistry can be discerned in the test results on temperature, efficiency, resistance and charge behaviour. However, the knowhow of the manufacturer appears often to be more deciding (Figs. 8 and 9). The influence of the multitude of factors like particle size and distribution, the exact formation of the passification layer and the addition of the so-called Black Magic (the numerous proprietary additives to improve both electrical and thermal conductivity, reduce flammability and suppress dendrite formation) cannot be neglected. Still conclusions can be drawn. The NMC cells have better efficiency and temperature performance than the other chemistries. The prismatic shape seems to have a clear negative effect on the efficiency and temperature. The tested NMC (pouch) cells have a better energy density and some LFP cells together with one NMC cell have the best pulse power density. The first is at least partly due to their high average cell potential; the latter is directly related to the allowed discharge rate by the manufacturer.

Depicting physical relationships behind cell properties can reveal effects that are invisible from the absolute value of the property. One cell (H) appears in this way to perform less well. The NiMH cell shows a higher efficiency loss if it is fully charged than the trend, pointing at side reactions in the cell. The indicator $R \times$ cap. appears to be important to understand cell behaviour. This indicator is not specifically biased by shape or chemistry.

Peculiar is that two cells are able to charge almost completely except some percents during the constant current phase (at 1 C). This shows the influence of optimising charge acceptance and conductivity through the cell. Assessing the charge behaviour of the cells is an addition in the applied enhanced test methodology that is ignored in the existing test methods.

According to the characterisation test plan consisting of four test methods, it is possible to classify 4 cells as initially best fitting with the intended applications and another 4 cells that might be considered for further testing, including lifetime tests.

References

[1] ESto Project Description & Public Results. www.flandersdrive.be/energy-storage

[2] ISO/DIS 12405-1 electrically propelled road vehicles – test specification for lithium-ion traction battery systems: high power applications, ISO, Switzerland, 2010.

[3] M.-S. Wu, P.-C.J. Chiang, J.-C. Lin, Y.-S. Jan, Correlation between electrochemical characteristics and thermal stability of advanced lithium-ion batteries in abuse tests – short-circuit tests, Electrochimica Acta 49 (2004) 1803.

[4] G. Mulder, N. Omar, S. Pauwels, F. Leemans, B. Verbrugge, W. De Nijs, P. Van den Bossche, D. Six, J. Van Mierlo, Enhanced test methods to characterise automotive battery cells, Journal of Power Sources 196 (2011) 10079.

[5] J. Axsen, A. Burke, K. Kurani, Batteries for plug-in hybrid electric vehicles (PHEVs): goals and state of the technology, Report UCDITS-RR-08-14, Institute of Transportation Studies, University of California, 2008.

[6] S. Abu-Sharkh, D. Doerffel, Rapid test and non-linear model characterization of solid-state lithium batteries, Journal of Power Sources 130 (2004) 266.

[7] K. Kato, A. Negishi, K. Nozaki, I. Tsuda, K. Takano, PSOC cycle testing method for lithium-ion secondary batteries, Journal of Power Sources 117 (2003) 118.

[8] A. Burke, M. Miller, Performance characteristics of lithium-ion batteries of various chemistries for plug-in hybrid vehicles, in: Proceedings EVS24, Norway, 2009.

[9] J.P. Fellner, G.J. Loeber, S.S. Sandhu, Testing of lithium-ion 18650 cells and characterizing/predicting cell performance, Journal of Power Sources 81–82 (1999) 867.

[10] J. Nguyen, Performance of phosphate lithium-ion batteries in motive applications, in: Proceedings of Battcon Conference, 2005.

[11] M. Smart, B.V. Ratnakumar, L.D. Whitcanack, F.J. Puglia, S. Santee, R. Gitzendanner, Life verification of large capacity Yardney Li-ion cells and batteries in support of NASA missions, International Journal of Energy Research 34 (2010) 116.

[12] C.E. Holland, J.W. Weidner, R.A. Dougal, R.E. White, Experimental characterization of hybrid power systems under pulse current loads, Journal of Power Sources 109 (2002) 32.

[13] N. Omar, M. Daowd, O. Hegazy, G. Mulder, J.-M. Timmermans, T. Coosemans, P. Van den Bossche, J. Van Mierlo, Standardization work for BEV and HEV applications: critical appraisal of recent traction battery documents, Energies 5 (2012) 138.

[14] IEC 62660-1 secondary batteries for electric road vehicles – performance testing for lithium-ion cells, 2010.

[15] Draft ISO/DIS 12405-2 electrically propelled road vehicles – test specification for lithium-ion traction battery systems: high energy application (draft in FDIS state, 2010), ISO, Switzerland, 2009.

[16] IEC 61982-2:2002 secondary batteries for the propulsion of electric vehicles – part 2. Dynamic discharge performance test and dynamic endurance test, IEC, Switzerland, 2002.

[17] FreedomCAR battery test manual for power assist hybrid electric vehicles, U.S. Department of Energy, U.S.A., 2003.

[18] Battery test manual for plug-in hybrid electric vehicles, U.S. Department of Energy, U.S.A., 2008.

[19] J. Yamaki, Secondary batteries – lithium rechargeable systems – lithium-ion – overview, in: J. Garche (Ed.), Encyclopedia of Electrochemical Power Sources, vol. 5, Elsevier, Oxford, 2009, p. 183.

[20] M. Wohlfahrt-Mehrens, C. Vogler, J. Garche, Aging mechanisms of lithium cathode materials, Journal of Power Sources 127 (2004) 58.

[21] J.W. Fergus, Recent developments in cathode materials for lithium ion batteries, Journal of Power Sources 195 (2010) 939.

[22] M. Broussely, P. Biensan, B. Simon, Lithium insertion into host materials: the key to success for Li ion batteries, Electrochimica Acta 45 (1999) 3.

[23] B. Scrosati, J. Garche, Lithium batteries: status, prospects and future, Journal of Power Sources 195 (2010) 2419.

[24] R. Lache, D. Galves, P. Nolan, Electric cars: plugged in – batteries must be included, Report by Deutsche Bank FITT Research, New York, 2008.

[25] N. Ravet, Y. Chouinard, J.F. Magnan, S. Besner, M. Gauthier, M. Armand, Electroactivity of natural and synthetic triphylite, Journal of Power Sources 97–98 (2001) 503.

[26] S.-Y. Chung, J.T. Bloking, Y.-M. Chiang, Electronically conductive phospho-olivines as lithium storage electrodes, Nature Materials 1 (2002) 123.

[27] S. Fletcher, Bottled Lightning: Superbatteries Electric Cars, and the New Lithium Economy, Hill & Wang, New York, 2011.

[28] K. Zaghib, A. Mauger, J.B. Goodenough, F. Gendron, C.M. Julien, Secondary batteries – lithium rechargeable systems – lithium-ion – positive electrode: lithium iron phosphate, in: J. Garche (Ed.), Encyclopedia of Electrochemical Power Sources, vol. 5, Elsevier, Oxford, 2009, p. 264.

[29] J. Zhu, K. Zeng, L. Lu, Cycling effects on surface morphology, nanomechanical and interfacial reliability of $LiMn_2O_4$ cathode in thin film lithium ion batteries, Electrochimica Acta 68 (2012) 52.

[30] D. Aurbach, Y. Talyosef, B. Markovsky, E. Markevich, E. Zinigrad, L. Asraf, J.S. Gnanaraj, H.-J. Kim, Design of electrolyte solutions for Li and Li-ion batteries: a review, Electrochimica Acta 50 (2004) 247.

[31] E. Krämer, R. Schmitz, S. Passerini, M. Winter, C. Schreiner, 1-Fluoropropane-2-one as SEI-forming additive for lithium-ion batteries, Electrochemistry Communications 16 (2012) 41.

[32] D. Doerffel, S.A. Sharkh, A critical review of using the Peukert equation for determining the remaining capacity of lead-acid and lithium-ion batteries, Journal of Power Sources 155 (2006) 395.

[33] J.L. Allen, J. Wolfenstine, K. Xu, D. Porschet, T. Salem, W. Tipton, W. Behl, J. Read, T.R. Jow, S. Gargies, Evaluation of Saft ultra high power lithium ion cells (VL5U), Army Research Laboratory, Public Report, U.S.A., 2009.

[34] M. Inaba, Secondary batteries – lithium rechargeable systems – lithium-ion – negative electrodes: graphite, in: J. Garche (Ed.), Encyclopedia of Electrochemical Power Sources, vol. 5, Elsevier, Oxford, 2009, p. 198.

[35] M.A. Fetcenko, et al., Recent advances in NiMH battery technology, Journal of Power Sources 165 (2007) 544.
[36] V. Svoboda, Batteries – fast charging, in: J. Garche (Ed.), Encyclopedia of Electrochemical Power Sources, vol. 1, Elsevier, Oxford, 2009, p. 424.
[37] A. Josse, W. Weydanz, Moderne Akkumulatoren Richtig Einsetzen, Inge Reichartverlag, Untermeitingen, Germany, 2006.
[38] Appendix D, FreedomCAR battery test manual for power assist hybrid electric vehicles, U.S. Department of Energy, U.S.A., 2003.